RSC Advances

PAPER

View Article Online
View Journal | View Issue



Cite this: *RSC Adv.*, 2020, **10**, 29385

# Fluorescence enhancement of quinolines by protonation†

Essi Tervola, [a] Khai-Nghi Truong, [a] Jas S. Ward, [a] Arri Priimagi [b] and Kari Rissanen *[a]

A study of the fluorescence enhancement of isoquinoline, acridine (benzo[*b*]quinoline) and benzo[*h*]quinoline is reported with six organic acids of different p$K_a$ values. Protonation was found to be an effective tool in the fluorescence enhancement of quinolines. A significant increase in the fluorescence intensity is observed only when strong acids are used, resulting in an over 50-fold increase in fluorescence with trifluoroacetic or benzenesulfonic acid and isoquinoline in a 1.5 : 1 ratio. The benzenesulfonic acid was found to be the most effective in the protonation of the bases despite its higher p$K_a$ value compared to trifluoro- and trichloroacetic acid. The X-ray crystal structures of 14 salts reveal the charge-assisted hydrogen bond O···N distances to vary very little, from 2.560(2)–2.714(3) Å, with the exception of the isoquinolinium benzenesulfonate where the O···N distance of 2.862(7) Å is caused by additional intermolecular interactions in the solid-state.

Received 27th May 2020
Accepted 23rd July 2020

DOI: 10.1039/d0ra04691d

rsc.li/rsc-advances



## Introduction

Supramolecular chemistry has been defined as "the chemistry of the intermolecular bond, covering the structures and functions of the entities formed by association of two or more chemical species".[1] The field of supramolecular chemistry has gained notable interest in the past decades due to its great potential in many subfields of molecular self-assembly, molecular recognition, and molecular machinery, all gaining advantage from non-covalent bonds.[2] Non-covalent interactions cover electrostatic, hydrogen-bonding, halogen-bonding, aromatic donor–acceptor, cation– and anion–π interactions, and solvophobic effects. Understanding the chemistry and intermolecular interactions of molecular entities and their associations provides significant advantages in the synthetic design of new systems, and are essential for understanding the world around us.

The importance of luminescence control is apparent not only in biological applications, *e.g.*, as a biosensing tool,[3] but also as an emission control in optical applications, such as lighting or organic light-emitting diodes.[4] A pH-dependent fluorescence has been reported in various occasions: de Silva *et al.* reported pH-dependent fluorescence of naphthalenic derivatives for molecular sensing and switching,[5,6] Ma *et al.* have reported pH-dependent fluorescent probes for cancer cell imaging,[7] and already decades ago Mataga *et al.* studied the hydrogen bonding effect on the fluorescence of some N-heterocycles.[8]

N-Heterocycles, such as quinolines, are known to be weakly fluorescent in comparison to their isoelectronic hydrocarbons. These heterocycles possess non-bonding electrons which give rise to (n–π*) excited states resulting in an increased spin–orbit coupling.[9–11] This coupling leads to an enhanced intersystem crossing, effectively decreasing the fluorescence quantum yield. It is also commonly observed that the protonation of the "aromatic" nitrogen results in a loss of emission fine structure and a notable red-shift in the emission wavelength.[12] Thus, studies of structurally simple N-heterocycles are vital for understanding further the effects of protonation on the emission of molecules.

The first report on the fluorescence of isoquinoline was recorded in frozen ethanol by Zimmermann and Joop nearly 50 years ago,[13] and later Ziegler and El-Sayed reported the phosphorescence of isoquinoline.[14] Additionally, the luminescence properties of nitrogen-containing heterocycles have been known to be strongly affected by the choice of solvent.[15] The excited-state proton transfer in N-heterocycles, including isoquinoline and benzo[*h*]quinoline, has been previously studied in acidic media.[9,16–18] Benzo[*h*]quinoline and acridine (benzo[*b*]quinoline), belonging to a group of polycyclic aromatic N-heterocycles, have been discovered to be particularly interesting since they possess different p$K_a$ values in the ground and excited state.[19–22] However, there has been no studies that are based on comparing different acids and the effects of the resulting counter-anion. The previous research in this area has

[a]*Department of Chemistry, University of Jyvaskyla, P.O. Box 35, Survontie 9B, 40014 Jyväskylä, Finland. E-mail: kari.t.rissanen@jyu.fi*

[b]*Smart Photonic Materials, Faculty of Engineering and Natural Sciences, Tampere University, P.O. Box 541, FI-33101 Tampere, Finland*

† Electronic supplementary information (ESI) available. CCDC 2000976–2000989. For ESI and crystallographic data in CIF or other electronic format see DOI: 10.1039/d0ra04691d

been scarce and focused on studying the emission of these compounds with a single base and, to the best of our knowledge, there are no reports of studies using single crystal X-ray diffraction to study the structural effects of protonation on these N-heterocycles.

Herein, we have compiled a comprehensive study on the effects of protonation on the fluorescence of three different quinolines using six different organic acids in solution and the structures of the resulting salts in the solid-state using single crystal X-ray diffraction.

## Results and discussion

The protonation of isoquinoline, acridine, and benzo[*h*]quinoline (see Scheme 1) was studied using absorption and fluorescence spectroscopy in dichloromethane (DCM, 0.5–1.0 $\times$ $10^{-4}$ M). The compounds were chosen due to their aromatic nature, commercial availability and the single site for protonation. The protonation was studied using six organic acids with different p$K_a$ values (see Scheme 2). Dichloromethane as an aprotic solvent was chosen to reduce the effects of solvation.

The full protonation of the base leads to an ion pair (a salt). An example of the protonation is depicted in Scheme 3 and investigated further in the following sections.

### Spectroscopic studies in solution

**Fluorescence studies.** The absorption and fluorescence spectra of isoquinoline titrated with trifluoroacetic acid (TFA) up to a 4 : 1 acid–base ratio are presented in Fig. 1 (for other acids, see ESI†). Based on the p$K_a$ value of 0.52,[24] TFA is the strongest acid used in the experiments. The natural absorbance of isoquinoline in DCM is shown in red. Isoquinoline has three slightly overlapping absorption bands at 268 nm, 305 nm, and 318 nm. As the protonation of the isoquinoline increases, the band at 268 nm decreases and experiences a bathochromic shift of 5 nm. During the protonation process, the band at 305 nm remains roughly the same and a new band arises at 328 nm. At 2.0 equivalents of the acid the spectrum shows saturation indicating a complete protonation of the base, as higher amounts of the acid do not induce any more spectral changes. Interestingly enough, based on the fluorescence spectra isoquinoline seems to be only 68% protonated with 1.0 equivalent of TFA.

The protonation of isoquinoline occurs in the ground state as deduced from the characteristics observed in the absorption spectrum. From the observed changes during the titration, the absorption at 268 nm can be assigned to the neutral species, whereas the band arising at 328 nm is assigned to the protonated species due to the ($\pi$,$\pi$*) transitions at longer wavelengths. Joshi *et al.* observed similar structureless broadband absorption in acidic medium at 330 nm for isoquinoline.[9] The absorption spectra of acridine and benzo[*h*]quinoline (see ESI†) show similar spectral changes at longer wavelengths due to protonation, but from these spectra, the absorption bands of the neutral and protonated species are difficult to distinguish. The smaller changes in the spectra could indicate that in those compounds, protonation occurs more easily in the excited state than in the ground state.[20]

The fluorescence intensity of isoquinoline increases significantly upon titration with acid. Similar to the absorption spectra, protonation induces an increase in the fluorescence intensity until the base is fully protonated. Isoquinoline and acridine (Fig. S4†) show only an increase in the intensity while the structure of the spectra remains the same. However, for benzo[*h*]quinoline a bathochromic shift of 50 nm of the fluorescence maxima of the neutral and the cationic species is observed. The absorption and fluorescence spectra of all the bases with different acids are presented in the ESI (see Fig. S1–S6).†

The absorption and fluorescence properties of aromatic N-heterocyclic compounds are strongly dependent on the properties of the solvent environment showing stronger fluorescence in polar solvents and weaker fluorescence in nonpolar solvents.[25a] In dichloromethane, isoquinoline itself is only weakly fluorescent due to its non-bonded electrons giving rise to an

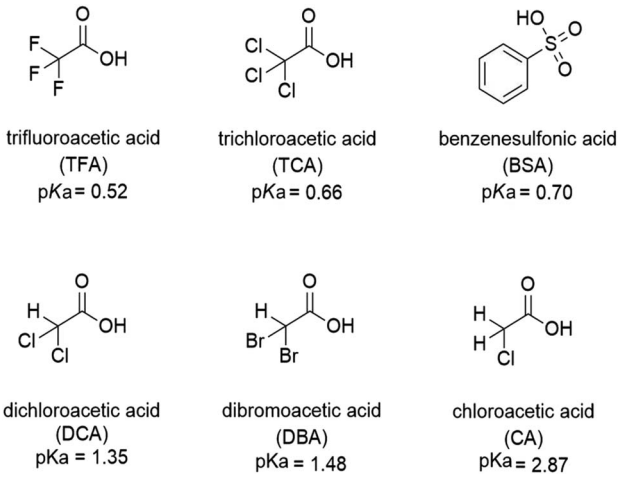


Scheme 2 The structures and p$K_a$ values of the acids used for the protonation of the bases.

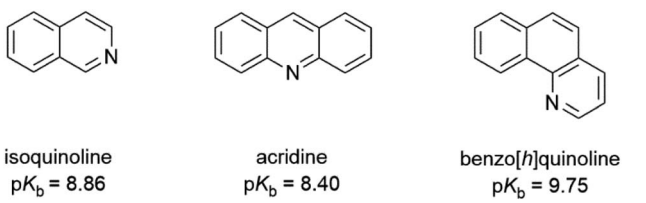


Scheme 1 The structures of isoquinoline, acridine, and benzo[*h*]quinoline used as bases and their p$K_b$ values in water.[23]

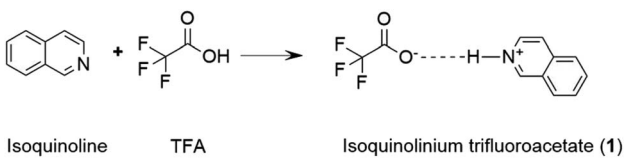


Scheme 3 The protonation of isoquinoline with trifluoroacetic acid resulting in the isoquinolinium trifluoroacetate salt.

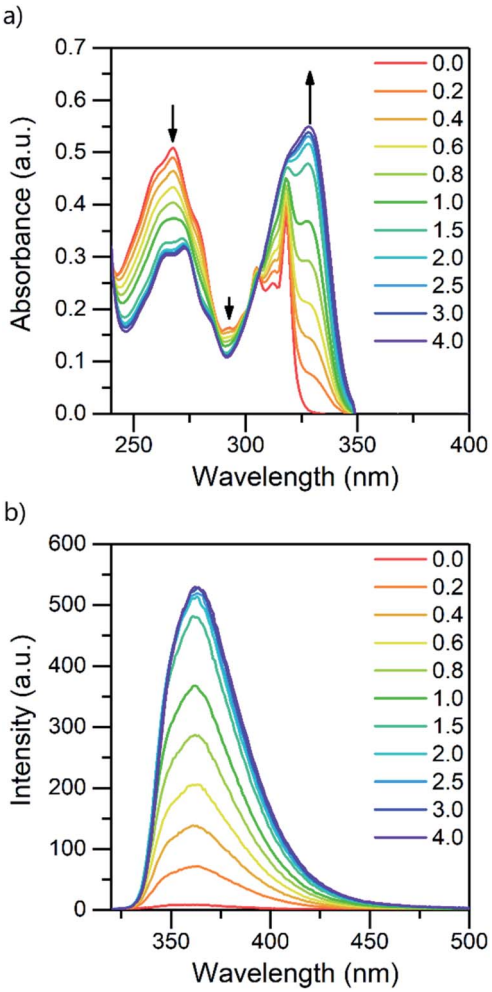


Fig. 1 Absorption (a) and fluorescence (b) spectra of isoquinoline while titrating with TFA from 0.0 to 4.0 equivalents of acid in DCM ($10^{-4}$ M, $\lambda_{ex}$ = 310 nm).

(n,π*) excited state.[26] The lone-pair of the nitrogen atom in the heterocyclic system interacts with the π-electrons restricting the freedom of the π-electrons and making the system π-deficient, and therefore restricting the fluorescence of the whole system.[27] Once the nitrogen gets protonated, the lone pair is shared with the hydrogen atom and the $S_1$ excited state is converted to a (π,π*) excited state resulting in a state more likely to undergo fluorescence which is observed as an increase in the fluorescence intensity. The fluorescence intensity increases until full protonation after which the intensity remains unchanged. Titration with TFA causes an over 50-fold increase in the fluorescence intensity of isoquinoline. Similar titrations were performed with all the acids shown in Scheme 2. Once the p$K_a$ value of the acid is higher than 1, the changes in fluorescence decrease significantly to an extent where chloroacetic acid (p$K_a$ = 2.87) induces virtually no changes to the fluorescence properties of isoquinoline due to insufficient donating power of the acid for protonation to occur. The fluorescence spectra of all studied quinolines treated with 1.0 equivalent of acid are presented in Fig. 2.

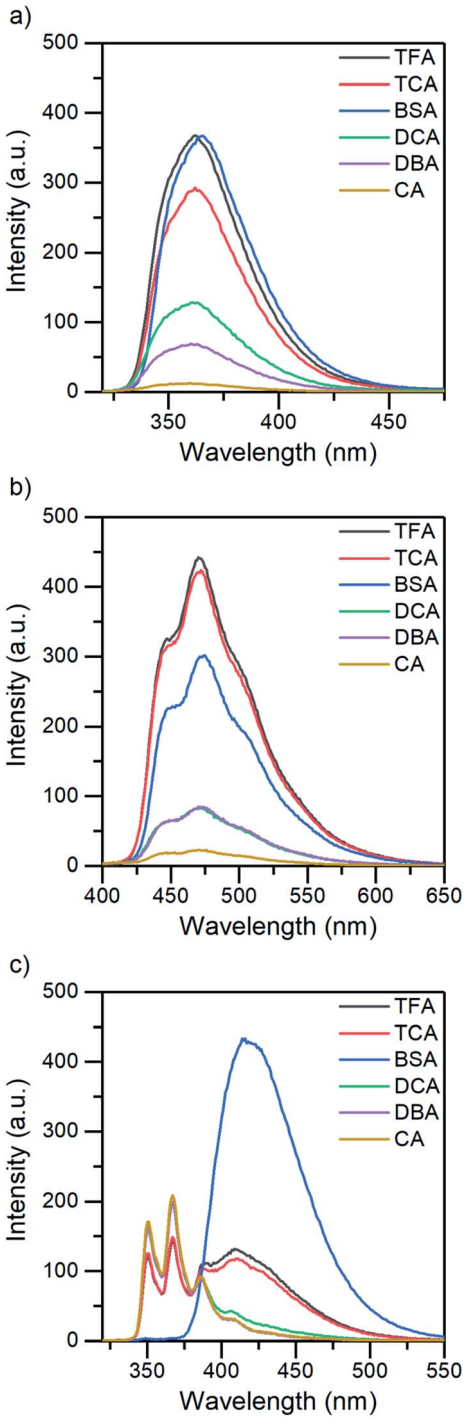


Fig. 2 The fluorescence spectra of (a) isoquinoline, (b) acridine, and (c) benzo[*h*]quinoline treated with 1.0 equivalent of acid in DCM ($5 \times 10^{-5}$ M, $\lambda_{ex}$ = 355 nm for acridine; and $10^{-4}$ M, $\lambda_{ex}$ = 310 nm for isoquinoline and benzo[*h*]quinoline).

**Determination of relative fluorescence intensity change and the fluorescence quantum yield.** Joshi *et al.* have previously reported excitation-dependent emission of isoquinoline in an aqueous medium where they distinguished structured fluorescence ($\lambda_{ex}$ = 310 nm) originating from a neutral species and broad emission at longer wavelengths ($\lambda_{ex}$ = 330 nm) due to

($\pi$,$\pi$*) transitions in a cationic species.[9] The changes in the spectra are dependent on the p$K_a$ value of the acid. The relative fluorescence intensities of the N-heterocycles become larger as the donating power of the acids increase resulting in more effective protonation. The relative intensity change can also be described as the fluorescence enhancement factor proportional to the acid addition. The change in the fluorescence intensity of the compounds was determined in relation to the native fluorescence of the compound. The changes in the fluorescence intensity of isoquinoline with all the acids are shown in Fig. 3a. The relative intensity change follows primarily the same trend with p$K_a$, excluding benzenesulfonic acid (BSA), the conjugate anion of which has much greater stability than the acetate anions. Due to the more stable anion, even though the p$K_a$ of BSA is higher, it is as effective in protonating the isoquinoline as TFA and similarly manifests an over 50-fold enhancement of the fluorescence intensity from the unprotonated isoquinoline. Similar results were obtained for acridine as well, with a maximum fluorescence enhancement factor of 25. For benzo[*h*]quinoline, the enhancement is not as significant for the fluorescence intensity since the neutral and cationic species emit in a very different wavelength and the fluorescence intensity experiences only a 5-fold increase with BSA (see ESI, Fig. S7†).

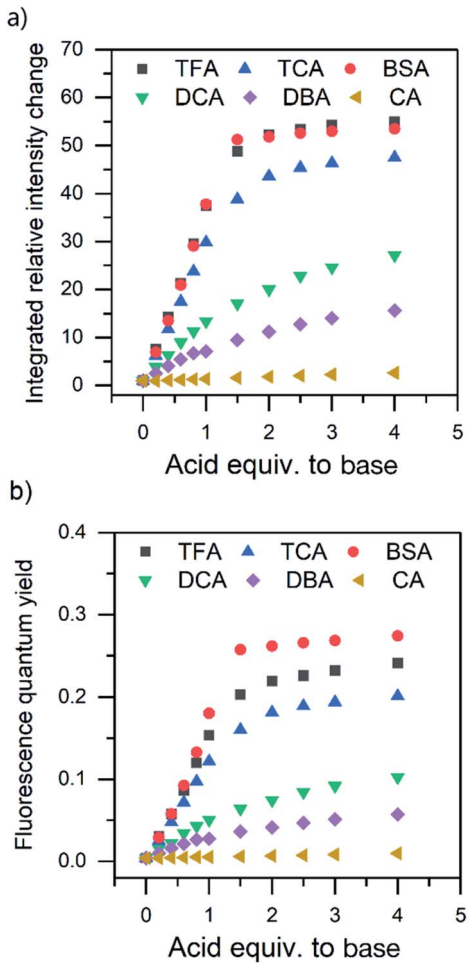


Fig. 3 (a) The integrated relative intensity change, and (b) the changes in the fluorescence quantum yield of isoquinoline while titrating with various acids (DCM, $10^{-4}$ M, $\lambda_{ex}$ = 310 nm, 0.0 to 4.0 acid equivalents).

The fluorescence quantum yield (QY) was studied using eqn (1)[25b] and 9,10-diphenylanthracene as reference ($\Phi_{FL}$ = 0.90, cyclohexane[28]).

$$\Phi = \Phi_{ref}\frac{\eta^2}{{\eta_{ref}}^2}\frac{I}{A}\frac{A_{ref}}{I_{ref}} \quad (1)$$

where $\Phi$ is the quantum yield, $\eta$ is the solvent refractive index, $I$ is the integrated fluorescence intensity and $A$ is the absorbance of the compound at the excitation wavelength.

Quantum yields for the quinolines in their native state were determined to be less than 1% for isoquinoline and acridine and 15% for benzo[*h*]quinoline. Again, by excluding BSA from the analysis, the QY evolution follows the trend of the p$K_a$ values. The greatest increase in QY can be observed for isoquinoline, changing from virtually zero to up to 27% (see Fig. 3b). The maximum fluorescence quantum yields obtained for all the compounds with each acid are listed in Table 1.

The change from the (n,$\pi$*) to ($\pi$,$\pi$*) excited state increases the fluorescence quantum yield. This is due to the (n,$\pi$*) states having longer radiative lifetimes than the ($\pi$,$\pi$*) states, and shorter lifetimes are more likely to undergo fluorescence before intersystem crossing.[26] However, the fluorescence quantum yield is defined as $\Phi_{FL} = 1 - \Phi_{ISC} - \Phi_{IC}$, where $\Phi_{ISC}$ is the phosphorescence quantum yield and $\Phi_{IC}$ is the quantum yield of internal conversion.

Isoquinoline experiences significant changes in its absorption spectra upon protonation. Distinctive absorption bands can be assigned to the neutral and cationic species differentiating isoquinoline from the other two N-heterocycles. Similar changes can be observed for acridine as well, merely to a smaller extent. Acridine has a different electronic structure leading to very narrow absorption bands and rendering the observation of the change and isosbestic points more challenging. As found for isoquinoline and acridine, the absorption of the cationic species can also be observed for benzo[*h*]quinoline at higher wavelengths, but contrary to isoquinoline and acridine, the absorption increases throughout the spectrum and no isosbestic points are observed.

In addition to that, benzo[*h*]quinoline also differs in terms of fluorescence: isoquinoline and acridine only experience an increase in their fluorescence intensity until eventually reaching

Table 1 Maximum fluorescence quantum yield ($\Phi_{FL}$) achieved for each base with different acids

| | Isoquinoline | Acridine | Benzo[*h*]quinoline |
|---|---|---|---|
| TFA | 0.241 | 0.089 | 0.157 |
| TCA | 0.201 | 0.082 | 0.156 |
| BSA | 0.274 | 0.101 | 0.148 |
| DCA | 0.102 | 0.035 | 0.157 |
| DBA | 0.057 | 0.031 | 0.156 |
| CA | 0.010 | 0.007 | 0.158 |
| Free base | 0.004 | 0.008 | 0.147 |

a saturation point, whereas the spectra of benzo[*h*]quinoline changes significantly. Neutral benzo[*h*]quinoline has a fluorescence maximum at 367 nm, whereas after protonation, the cationic species arises at 416 nm, shifting the fluorescence maximum 50 nm and changing the spectra from three distinctive bands to one broadband fluorescence. These drastic changes affect the overall fluorescence intensity change making it minuscule in comparison to the isoquinoline and acridine 50-fold and 25-fold increases, respectively.

All three compounds also share similarities in their fluorescence intensity. The intensity changes vary between the compounds, but in each case, BSA has the largest effects, while the acetic acids follow the trend of their respective p$K_a$ values. Considering the chemical structure of benzo[*h*]quinoline, it is apparent that it is more prone to steric hindrance than isoquinoline and acridine due to the hydrogen at C10 (see ESI, Fig. S35†) which causes a severe clash with the hydrogen at the nitrogen atom during the protonation.

**Determination of the binding constants.** Isoquinoline, acridine, and benzo[*h*]quinoline have been classified as having p$K_b$ values of 8.86, 8.40, and 9.75, respectively.[23] For isoquinoline, the protonation saturation is observed with all the stronger acids (TFA, TCA, and BSA), but in variable ratios (2.0, 2.5 and 1.5, respectively). Using BSA, the saturation is observed in the fluorescence spectra for isoquinoline at 1.5 equivalents, whereas for acridine this occurs at 2.5, and for benzo[*h*]quinoline at 1.0, the latter indicating easier protonation than for isoquinoline and acridine. The above-presented differences in the protonation efficiency can be explained by the difference of the p$K_b$ values in the ground state and the excited state of the base. From the absorption and fluorescence spectra, it can be concluded that benzo[*h*]quinoline, like its isomer benzo[*f*]quinoline,[20] is more readily protonated in the excited state.

Due to the unsuitability of the NMR spectroscopy (see ESI, Fig. S11–S14†) for binding constant determination, the absorption and fluorescence spectra of the bases were used instead. Due to the difficulty in determining pH values in DCM, the binding constants were determined only for isoquinoline, for which the absorbance of the neutral and cationic species could be easily determined from the absorption spectrum. For isoquinoline, the absorption band at 268 nm signifies the absorbance of the neutral species, which decreases upon addition of the acids, whereas the band at 328 nm is contributed by the cationic species (see Fig. 4). These changes can be used to determine the ratio of *c*(bound) and *c*(unbound). Binding constants for the ground state are determined using eqn (2)[29]

$$\frac{c(\text{bound})}{c(\text{unbound})} = K_a[\text{Q}] \quad (2)$$

where $K_a$ is the binding constant for the protonation of the base and [Q] is the concentration of the added acid. The intensity changes at 268 and 328 nm and their ratio during titration with TFA are presented in Fig. 4. Binding constants can be determined from the linear fit of the two bands designated to the two different species. It should be noted that for all the compounds, the titration points exceeding the saturation limit were excluded from the fit. For some of the spectra, the changes were insignificant, and the binding constants could not be determined

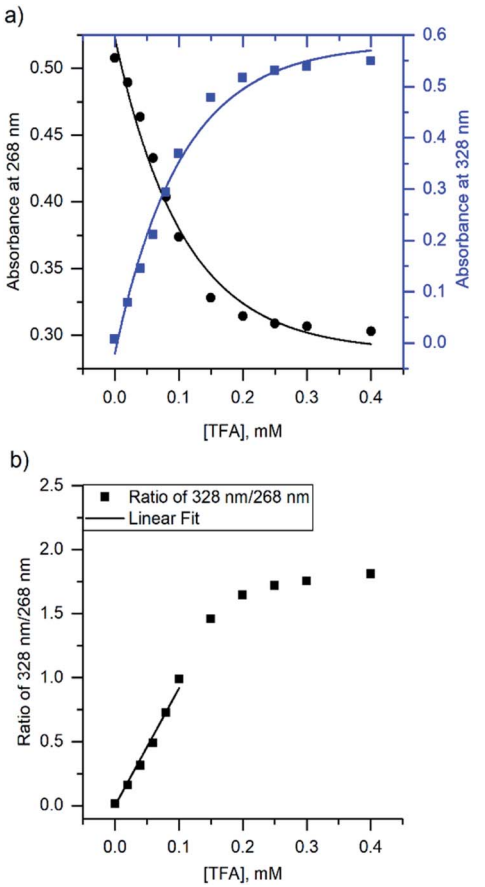


Fig. 4 (a) The change in absorbance of isoquinoline at 268 nm and 328 nm upon addition of TFA, and (b) ratio of the intensities at 268 nm and 328 nm with linear fit.

using this method. The determined binding constants are listed in Table 2.

The binding constant for the protonation of isoquinoline with CA was not determined simply because the changes in the spectra are too small and within experimental error. The determined binding constants (see ESI, S9 and S10†) obey the trend of the p$K_a$ values of the acids yet again excluding BSA, which has a significantly higher binding constant for isoquinoline than the other acids. Although the binding constants for acridine and benzo[*h*]quinoline were not determined, similar results are expected based on the fluorescence spectra.

Table 2 Binding constants ($K_a$) for the protonation of isoquinoline in the ground state determined from the absorption spectra according to eqn (2).[29]

| | $K_a$ ($M^{-1}$) |
|---|---|
| TFA | 9200 ± 330 |
| TCA | 8300 ± 190 |
| BSA | 32 700 ± 1590 |
| DCA | 4000 ± 100 |
| DBA | 3100 ± 120 |
| CA | N/A |

Table 3 Nomenclature of the obtained single crystals

| | TFA | TCA | BSA | DCA | DBA | CA |
|---|---|---|---|---|---|---|
| Isoquinoline | 1 | 2 | 3 | — | — | — |
| Acridine | 4 | 5 | 6 | 7 | 8 | 9 |
| Benzo[*h*]quinoline | 10 | 11 | 12 | 13 | 14 | — |

## Single crystal X-ray crystallography

The crystallizations of the acid–base pairs were carried out with 1 : 1 acid–base ratio in chloroform and the single crystals of the corresponding salts were obtained either by slow evaporation of the chloroform solution or by vapor diffusion using chloroform/hexane or dichloromethane/diisopropyl ether as the solvent/antisolvent system. Unfortunately, not all of the crystallizations were successful and some of the salts from weaker acids were obtained as a gel or amorphous powder. The suitable single crystals were subjected to single crystal X-ray study. To simplify the crystallographic nomenclature, the salts are referred to as numbers, *e.g.* isoquinolinium trifluoroacetate is denoted as **1**. The numbering of all the salts is shown in Table 3.

The salt formation, *viz.* full protonation of isoquinoline, acridine, and benzo[*h*]quinoline, was observed in the solid-state in all cases, regardless of the p$K_a$ values of the used acid. All solid-state structures, except **7**, **8**, **13** and **14**, have the expected

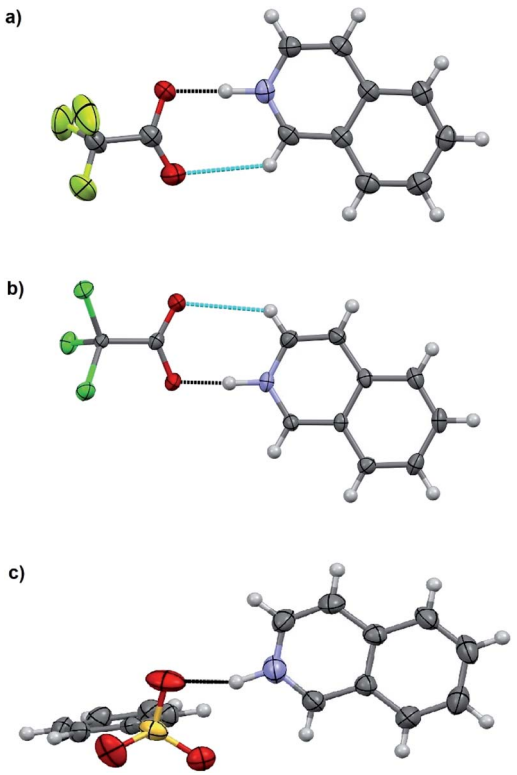


Fig. 5 X-ray structures of (a) **1**, (b) **2**, and (c) **3**. Displacement ellipsoids are drawn at the 50% probability level. The black-dotted lines are the N–H···O hydrogen bonds and the blue-dotted lines represent weak C–H···O interactions.

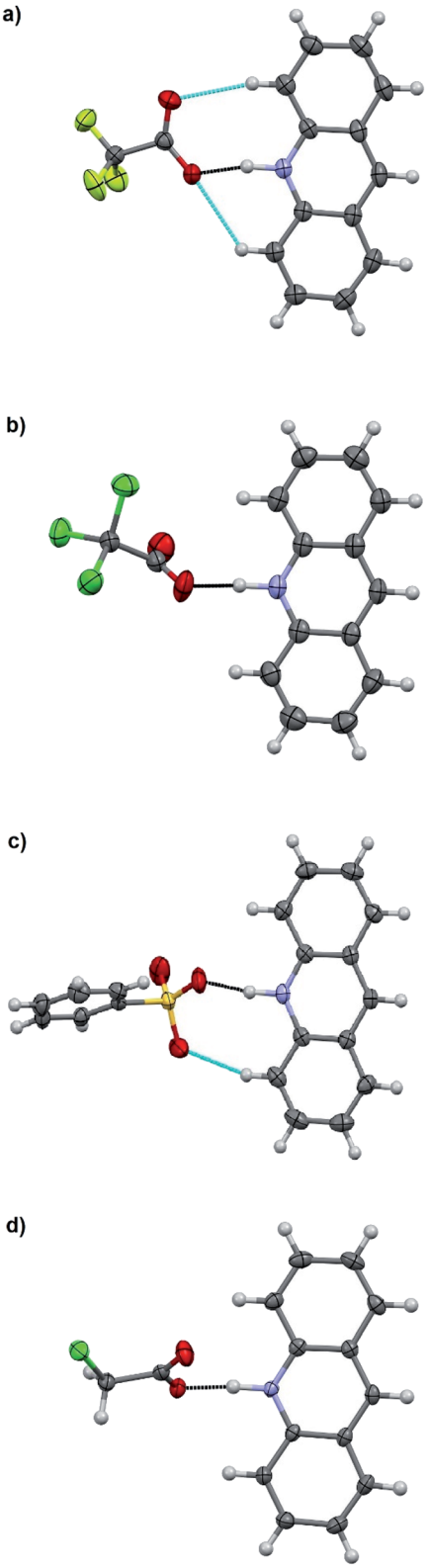


Fig. 6 X-ray structures of (a) **4**, (b) **5**, (c) **6**, and (d) **9**. Displacement ellipsoids are drawn at the 50% probability level. The black-dotted lines are the N–H···O hydrogen bonds and the blue-dotted lines represent C–H···O interactions.

1 : 1 stoichiometry (see Fig. 5 and 6). The deprotonated acid dimer (R–COOH···OOC–R) found in **7**, **8**, **13** and **14** is H-bonded to the H–$N^+$ moiety from the deprotonated acid, unlike in the

 

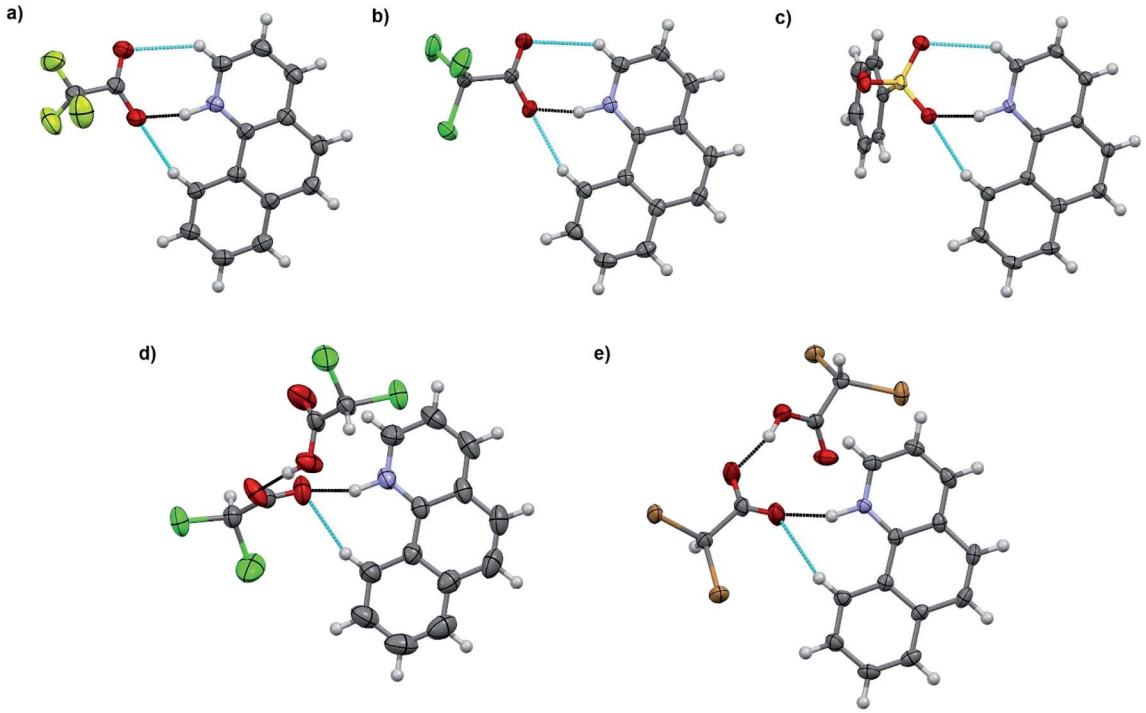


Fig. 7 X-ray structures of (a) **10**, (b) **11**, (c) **12**, (d) **13**, and (e) **14**. Displacement ellipsoids are drawn at the 50% probability level. The black-dotted lines are the N–H···O hydrogen bonds and the blue-dotted lines represent weak C–H···O interactions.

other studied structures, and has formally a 2 : 1 stoichiometry (see Fig. 7).

The charge-assisted hydrogen bond distances between the corresponding acetate or sulfonate oxygen and the nitrogen of the protonated base (O···N) are listed in Table 4. Due to the unreliable positioning of the hydrogen atom from X-ray data, only the distances between the heavier atoms (O and N) are discussed. However during the refinements, a realistic H–N bond distance of 1.04 Å, based on an average of neutron diffraction values,[30] was used.

The charge-assisted H-bond distances for TFA and TCA (**1**, **2**, **4**, **5**, **10**, and **11**) salts are very close to each other ($\Delta\delta = 0.02$–$0.05$ Å). From the solution studies (see above), it was concluded that the protonation of isoquinoline by BSA was the most effective as it had the greatest effect on the fluorescence intensity and induced the largest chemical shift change in the $^1$H NMR spectra (see ESI,† NMR studies). Yet in the solid-state, the O···N distance for 3 is found to be the longest, 2.862(7) Å, being 0.245–0.148 Å longer than for **1**, **2**, **6** or **12**. The plausible explanation for the longer O···N distance in the BSA–isoquinoline salt are the slightly acidic H-atoms of the phenyl ring of the benzenesulfonate anion, resulting in a multitude of additional H-bonds to the adjacent anions, and thus elongating the charge-assisted N–H···O–S hydrogen bond. The same phenomenon does not occur in the corresponding acridine (**6**) and benzo[*h*]quinoline (**12**). This is evidenced by the Hirshfeld surface analysis of **3**, **6** and **12** (see ESI, Fig. S45†) which clearly indicates a multitude of H···O interactions to adjacent benzenesulfonate anions only in the case of **3**. The DFT-level (SPARTAN18,[31] M062X, def2-TZVP, nonpolar solvent model) calculations for **3**, **6** and **12** also support this reasoning, as all optimized structures give the nonpolar solvent phase O···N distances between 2.6–2.7 Å (see ESI, Fig. S46†).

The acridinium cation in the DCA and DBA salts (**7** and **8**, see Fig. S27–S32,† respectively) reside on a symmetry element resulting in disorder of the $^+$N–H and C–H parts of the acridine skeleton. This is manifested by the abnormally long O···N distances, as they actually represent the average of the 2.7 Å ($^+$N–H···O$^-$) and 3.5 Å (C(arom)–H···O) distances, thus these XRD based distances for **7** and **8** are excluded from the discussion. The same DFT-level (SPARTAN18,[31] M062X, def2-TZVP, nonpolar solvent model) calculations for **7** and **8** confirm the normal solution phase O···N distances to be 2.6 Å (see ESI, Fig. S47†). In contrast to the 1 : 1 salts, the structures of **7** and **8** are formed in a 2 : 1 ratio in the solid-state, consisting of one

Table 4 The charge-assisted hydrogen bond O···N distances for the salts [Å]

| | Isoquinoline | Acridine | Benzo[*h*]quinoline |
|---|---|---|---|
| TFA | **1**: 2.645(4) | **4**: 2.636(2) | **10**: 2.644(3) |
| TCA | **2**: 2.617(4) | **5**: 2.617(3) | **11**: 2.633(4)[a], **11**: 2.634(4)[a] |
| BSA | **3**: 2.862(7) | **6**: 2.666(3) | **12**: 2.714(3) |
| DCA | Gel | **7**: 3.031(4)[b] | **13**: 2.657(3) |
| DBA | Gel | **8**: 3.102(6)[b] | **14**: 2.709(6) |
| CA | Gel | **9**: 2.560(2) | Powder |

[a] Two independent 1 : 1 acid–base pairs in the asymmetric unit. [b] Acridine moiety is disordered over a symmetry element resulting in unreliable O···N distances.

(disordered) acridinium cation and a H-bonded DCA or DBA dimer (see ESI, Fig. S27 and S28†). Similar acid dimers in a 2 : 1 acid–base ratio were observed for benzo[*h*]quinoline with DCA (**13**) and DBA (**14**), respectively. Yet, due to the non-disordered structures of **13** and **14**, the O···N distances are very similar to the 1 : 1 salts (see Table 4). Surprisingly, the shortest O···N interaction distance is observed in **9** with 2.560(2) Å which is even 0.03 Å shorter than in the reported quinolinium trifluoroacetate structure,[32] and very close to the DFT-level (SPARTAN18,[31] M062X, def2-TZVP, nonpolar solvent model) calculated O···N distance of 2.61 Å for **9** (see ESI, Fig. S47†).

A search in the Cambridge Structural Database (CSD)[33] for protonated isoquinoline, acridine and benzo[*h*]quinoline resulted in 22 hits, respectively. The average charge-assisted hydrogen bond O···N distance calculated from the CSD structures[34–47] is 2.658 Å, precisely matching the average of 2.644 Å calculated from **1**, **2**, **4**, **5**, **6**, **9**, **10**, **11**, **12**, **13** and **14** (excluding the abnormally long O···N distances in **3**, **7** and **8**).

## Conclusions

The protonation of simple N-heterocycles was successfully used as a preliminary study to gain further information on the use of acid–base interactions for supramolecular emission control. The protonation was found to significantly boost fluorescence emission, hence being an effective tool to be used in fluorescence enhancement and avoiding time-consuming synthetic procedures. In the solution studies, the protonation was observed to increase the fluorescence intensity with an over 50-fold increase observed for isoquinoline. Surprisingly, the protonation was found to be incomplete in a 1 : 1 acid–base ratio, despite the single protonation site of the bases. No structural changes were observed in the fluorescence spectra of isoquinoline or acridine, but interestingly, benzo[*h*]quinoline experiences a bathochromic shift of 50 nm upon protonation. Benzo[*h*]quinoline and acridine were also observed to be more easily protonated in the excited state than in the ground state, whereas the isoquinoline absorption spectra display effective protonation in the ground state.

The relative fluorescence intensities of the N-heterocycles become larger as the donating powers of the proton donors increase. The increase in the fluorescence intensity followed the same trend with the p$K_a$ values of the acids with the exception of BSA, which was the most effective in protonating all the bases. Acids with p$K_a$ values higher than 1 did not have significant effects on the fluorescence of the compounds due to insufficient donating power of the acid for protonation to occur. Binding constants for isoquinoline in the ground state were determined based on the absorption spectra and similar results were observed in these values as well, with BSA having a three times larger binding constant compared to the other, stronger acids (TFA and TCA).

In the solid-state, the protonation of isoquinoline, acridine and benzo[*h*]quinoline was observed in each case regardless of the p$K_a$ value of the acid. In solution, BSA was determined to be the most effective in the protonation of the bases, yet, in single-crystal X-ray structures, the O···N distance was found to be the longest in the BSA–isoquinoline salt due to additional intermolecular interactions in the solid-state. The solid-state studies suggested that the O···N distances were mainly affected by the lattice interactions and do not directly reflect the acid–base or the anion–cation interactions in solution.

## Conflicts of interest

There are no conflicts to declare.

## Acknowledgements

We gratefully acknowledge financial support from the Academy of Finland (KR: grant no. 317259; AP: grant no. 311142) and the University of Jyväskylä, Finland.

## Notes and references

1 J. M. Lehn, *Angew. Chem., Int. Ed. Engl.*, 1988, **27**, 89–112.
2 J. Steed and J. Atwood, *Supramolecular Chemistry*, John Wiley & Sons Ltd., Chippenham, United Kingdom, 2009.
3 S. Vigneshvar, C. C. Sudhakumari, B. Senthilkumaran and H. Prakash, *Front. Bioeng. Biotechnol.*, 2016, **4**, 11.
4 J.-H. Lee, C.-H. Chen, P.-H. Lee, H.-Y. Lin, M.-K. Leung, T.-L. Chiu and C.-F. Lin, *J. Mater. Chem. C*, 2019, **7**, 5874–5888.
5 A. P. de Silva, A. Goligher, N. Gunaratne and T. E. Rice, *ARKIVOC*, 2003, **7**, 229–243.
6 S. Zheng, P. L. M. Lynch, T. E. Rice, T. S. Moody, H. Q. N. Gunaratne and A. P. de Silva, *Photochem. Photobiol. Sci.*, 2012, **11**, 1675–1681.
7 J. Ma, W. Li, J. Li, R. Shi, G. Yin and R. Wang, *Talanta*, 2018, **182**, 464–469.
8 N. Mataga and S. Tsuno, *Bull. Chem. Soc. Jpn.*, 1957, **30**, 368–374.
9 N. K. Joshi, H. C. Joshi, R. Gahlaut, N. Tewarj, R. Rautela and S. Pant, *J. Phys. Chem. A*, 2012, **116**, 7272–7278.
10 N. Mataga, *Bull. Chem. Soc. Jpn.*, 1958, **31**, 459–462.
11 M. F. Anton and W. R. Moomaw, *J. Chem. Phys.*, 1977, **66**, 1808–1818.
12 S. A. Tucker, W. E. Acree Jr and C. Upton, *Polycyclic Aromat. Compd.*, 1993, **3**, 221–229.
13 H. Zimmermann and N. Joop, *Z. Elektrochem.*, 1961, **65**, 61–66.
14 S. M. Ziegler and M. A. El-Sayed, *J. Chem. Phys.*, 1970, **52**, 3257–3268.
15 I. Janic and A. Kawski, *Adv. Mol. Relax. Processes*, 1973, **5**, 185–191.
16 K. Kumari, N. Tewari, M. S. Mehta, N. Pandey, K. Tiwari, R. K. Ratnesh, H. C. Joshi and S. Pant, *J. Mol. Struct.*, 2019, **1180**, 855–860.
17 M. Norek, J. Dresner and J. Prochorow, *Acta Phys. Pol., A*, 2003, **104**, 425–439.
18 M. Norek, B. Kozankiewicz and J. Prochorow, *Acta Phys. Pol., A*, 2004, **106**, 77–94.
19 E. T. Ryan, T. Xiang, K. P. Johnston and M. A. Fox, *J. Phys. Chem. A*, 1997, **101**, 1827–1835.

 

20 M. Nakamizo, *Spectrochim. Acta*, 1966, **22**, 2039–2053.
21 A. Grabowska, B. Pakula and J. Pancir, *Photochem. Photobiol.*, 1969, **10**, 415–425.
22 E. Vander Donckt, R. Dramaix, J. Nasielski and C. Vogels, *Trans. Faraday Soc.*, 1969, **65**, 3258–3262.
23 H. C. Brown, *et al.*, in *Determination of Organic Structures by Physical Methods*, ed. E. A. Braude, and F. C. Nachod, Academic Press, New York, 1955.
24 Acid Dissociation Constants, *CRC Handbook of Chemistry and Physics*, retrieved on 20.12.2018.
25 (*a*) B. Valeur, *Molecular Fluorescence: Principles and Applications*, Wiley-VCH Verlag GmbH, New York, 2001, p. 59; (*b*) B. Valeur, *Molecular Fluorescence: Principles and Applications*, Wiley-VCH Verlag GmbH, New York, 2001, p. 161.
26 B. Wardle, *Principles and Applications of Photochemistry*, John Wiley & Sons, Ltd., United Kingdom, 2009.
27 R. T. Williams and J. W. Bridges, *J. Clin. Pathol.*, 1964, **17**, 371–394.
28 D. F. Eaton, *Pure Appl. Chem.*, 1988, **60**, 1107–1114.
29 G. Grynkiewicz, M. Poenie and R. Tsien, *J. Biol. Chem.*, 1985, **260**, 3440–3450.
30 F. H. Allen and I. J. Bruno, *Acta Crystallogr., Sect. B: Struct. Sci.*, 2010, **66**, 380–386.
31 *SPARTAN18*, Wavefunction Inc., Irvine, CA, USA, 2018.
32 Effendy, P. C. Junk, C. J. Kepert, L. M. Louis, T. C. Morien, B. W. Skelton and A. H. White, *Z. Anorg. Allg. Chem.*, 2006, **632**, 1312–1325.
33 C. R. Groom, I. J. Bruno, M. P. Lightfoot and S. C. Ward, *Acta Crystallogr., Sect. B: Struct. Sci., Cryst. Eng. Mater.*, 2016, **72**, 171–179.
34 X.-H. Chang, *Z. Kristallogr. – New Cryst. Struct.*, 2019, **234**(6), 1253–1254.
35 N. Kobayashi, T. Naito and T. Inabe, *Bull. Chem. Soc. Jpn.*, 2003, **76**, 1351–1362.
36 H. Eshtiagh-Hosseini, A. Hassanpoor, M. Mirzaei and A. R. Salimi, *Acta Crystallogr., Sect. E: Struct. Rep. Online*, 2010, **66**, o2996.
37 P. Bora, B. Saikia and B. Sarma, *Cryst. Growth Des.*, 2018, **18**(3), 1448–1458.
38 L. Plasseraud and H. Cattey, *C. R. Chim.*, 2013, **16**, 613–620.
39 H. Aghabozorg, J. A. Gharamaleki, M. Parvizi and Z. Derikvand, *Acta Crystallogr., Sect. E: Struct. Rep. Online*, 2010, **66**, m83–m84.
40 N. Bedekovic, V. Stilinovi and T. Piteša, *Cryst. Growth Des.*, 2017, **17**, 5732–5743.
41 X. Mei and C. Wolf, *Eur. J. Org. Chem.*, 2004, 4340–4347.
42 Z. Derikvand, M. M. Olmstead and J. A. Gharamaleki, *Acta Crystallogr., Sect. E: Struct. Rep. Online*, 2011, **67**, o416.
43 K. Fennig and A. Sikorski, *Z. Kristallogr. – New Cryst. Struct.*, 2018, **233**(4), 675–676.
44 P. P. Devi and D. Kalaivani, *Acta Crystallogr., Sect. B: Struct. Sci., Cryst. Eng. Mater.*, 2016, **72**, 570–574.
45 D. E. Lynch, A. N. Kirkham, M. Z. J. Chowdhury, E. S. Wane and J. Heptinstall, *Dyes Pigm.*, 2012, **94**, 393–402.
46 A. Garai, S. Mukherjee, S. K. Ray and K. Biradha, *Cryst. Growth Des.*, 2018, **18**, 581–586.
47 E.-Y. Xia, J. Sun, R. Yao and C.-G. Yan, *Tetrahedron*, 2010, **66**, 3569–3574.